Structure and crystallization of rapidly quenched Cu–(Zr or Hf)–Ti alloys containing nanocrystalline particles

2002 J. Phys.: Condens. Matter 14 13867

(http://iopscience.iop.org/0953-8984/14/50/312)

INSTITUTE OF PHYSICS PUBLISHING JOURNAL OF PHYSICS: CONDENSED MATTER

J. Phys.: Condens. Matter **14** (2002) 13867–13877 PII: S0953-8984(02)39308-1

Structure and crystallization of rapidly quenched Cu–(Zr or Hf)–Ti alloys containing nanocrystalline particles

M Kasai[1,4], **J Saida**[1,5], **M Matsushita**[2], **T Osuna**[3], **E Matsubara**[3] and **A Inoue**[3]

[1] Inoue Superliquid Glass Project, ERATO, Japan Science and Technology Corporation (JST), Yagiyamaminami 2-1-1, Sendai 982-0807, Japan
[2] JEOL Ltd, Akishima, Tokyo 156-8558, Japan
[3] Institute for Materials Research, Tohoku University, Sendai 980-8577, Japan

E-mail: jsaida@imr.tohoku.ac.jp

Received 10 July 2002
Published 6 December 2002
Online at stacks.iop.org/JPhysCM/14/13867

Abstract

The structure and primary crystallization process of the melt-spun $Cu_{60}(Zr\ or\ Hf)_{30}Ti_{10}$ alloys were investigated. Compositional segregation in the diameter range of 5–10 nm was observed in the as-quenched state. In the high-resolution transmission electron microscopy images, nanocrystalline particles are observed in the glassy matrix, the size of which corresponds to the scale of compositional segregation. The glassy region has comparatively high Zr or Hf and Ti contents. In contrast, the Cu element is enriched in the nanocrystalline phases. The nanocrystalline phases are identified as the cubic structure with a lattice constant of approximately 0.5 nm. These results are recognized as the formation of novel structure consisting of the glassy and nanocrystalline phases. It is suggested that the precipitation of body-centred-cubic CuZr phase as a primary crystallization phase proceeds in the glassy phase, the nanocrystalline phase remaining in the Cu–Zr–Ti alloy. Meanwhile, the glassy and nanocrystalline phases are transformed to an orthorhombic Cu_8Hf_3 phase in the initial crystallization stage in the Cu–Hf–Ti alloy.

1. Introduction

Recently, new Cu-based bulk glassy alloys with high mechanical strength have been reported in the Cu–(Zr and Hf)–Ti systems [1]. These bulk glassy alloys have attracted attention in the fact that they do not satisfy the three empirical rules for high glass-forming ability (GFA), which has applied to most bulk glassy alloys in various systems. The rules are described as

[4] Present address: Kawasaki Steel Co. Ltd, Chiba 260-0835, Japan.
[5] Address for correspondence: Institute for Materials Research, Tohoku University, Sendai 980-8577, Japan.

(1) a multicomponent system consisting of more than three elements,
(2) atomic size mismatches more than 12% and
(3) large negative heat of mixing among the major constitutional elements [2].

In the ternary Cu–Zr–Ti system, for example, the atomic size of the constitutional elements is in the order of Zr > Ti > Cu and the atomic ratios are 1.28 for Zr/Cu, 1.10 for Zr/Ti and 1.14 for Ti/Cu, which indicates a small size mismatch between the Zr–Ti and Ti–Cu pairs. Furthermore, heats of mixing have been estimated to be -23 kJ mol^{-1} for Cu–Zr, 0 kJ mol^{-1} for Zr–Ti and -9 kJ mol^{-1} for Cu–Ti [3]. These values of negative heats of mixing are smaller than those among the atomic pairs in the typical alloys with high GFA such as Zr–Al–Cu and Zr–Al–Ni systems, for example [4, 5] and it is noted that the Zr–Ti pair has no chemical affinity in the Cu–Zr–Ti system. Similar tendencies are confirmed in the Cu–Hf–Ti alloy. These facts are expected to create a novel structure in the glassy state in the Cu–(Zr and Hf)–Ti alloys. It is also expected that the local atomic structure in the as-quenched state and the transformation behaviour are different from those in the previously reported bulk-forming metallic glasses [6, 7]. In this paper, we examine the structure of the melt-spun Cu_{60}(Zr or Hf)$_{30}$Ti$_{10}$ alloys using x-ray diffraction (XRD) and transmission electron microscopy (TEM) in order to investigate the feature of the novel structure in these alloys. Moreover, we report the primary crystallization processes of these alloys.

2. Experimental procedure

Melt-spun Cu_{60}(Zr or Hf)$_{30}$Ti$_{10}$ ternary alloys with a cross section of 0.03×1 mm^2 were produced from alloy ingots prepared by arc melting high-purity metals of 99.999 mass% Cu, 99.9 mass% Zr, 99.9 mass% Hf and 99.9 mass% Ti in a purified argon atmosphere. The local atomic structure of the melt-spun alloys was studied by ordinary XRD with monochromatic Mo Kα radiation operated at 50 kV–200 mA produced by a molybdenum rotary x-ray target and a single-flat graphite monochromator. The observed intensity was corrected for air scattering, polarization and absorption, and converted to electron units per atom by the Krogh–Moe–Norman method [8] to obtain the interference function $Qi(Q)$ estimated from the coherent scattering intensity in absolute units. The ordinary radial distribution function (RDF), $2\pi r^2\rho(r)$, was computed by Fourier transformation of $Qi(Q)$. Local atomic structures around each element (environmental RDFs) were determined by the anomalous x-ray scattering (AXS) measurements [9, 10] at Zr Kα and Cu Kα absorption edges in the $Cu_{60}Zr_{30}Ti_{10}$ alloy. The AXS measurements were carried out at BL-9C in the Photon Factory of the Institute of Materials Structure Science (IMSS), High-Energy Accelerator Research Organization (KEK), Tsukuba, Japan. The structure was also examined by high-resolution transmission electron microscopic (HREM) observation using field-emission transmission electron microscopy (FE-TEM) with an accelerating voltage of 300 kV (JEOL JEM-3000F). The sample for TEM observation was prepared by the ion milling technique with liquid nitrogen cooling. The compositional analysis was performed by nanobeam energy dispersive x-ray spectroscopy (EDX) and high-angle annular detector dark-field scanning transmission electron microscopy (HAADF-STEM).

3. Results and discussion

3.1. Structure in the as-quenched state

Figures 1 and 2 show XRD patterns and DSC curves, respectively, of the melt-spun $Cu_{60}Zr_{30}Ti_{10}$ and $Cu_{60}Hf_{30}Ti_{10}$ alloys. No obvious diffraction peaks are observed in either

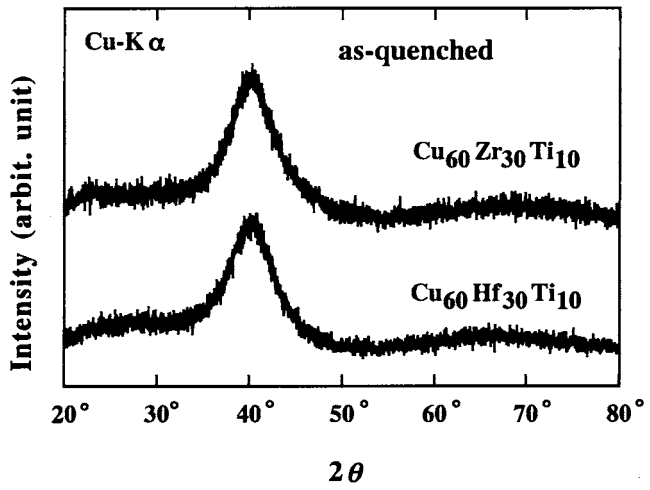

Figure 1. XRD patterns of the melt-spun $Cu_{60}Zr_{30}Ti_{10}$ and $Cu_{60}Hf_{30}Ti_{10}$ alloys.

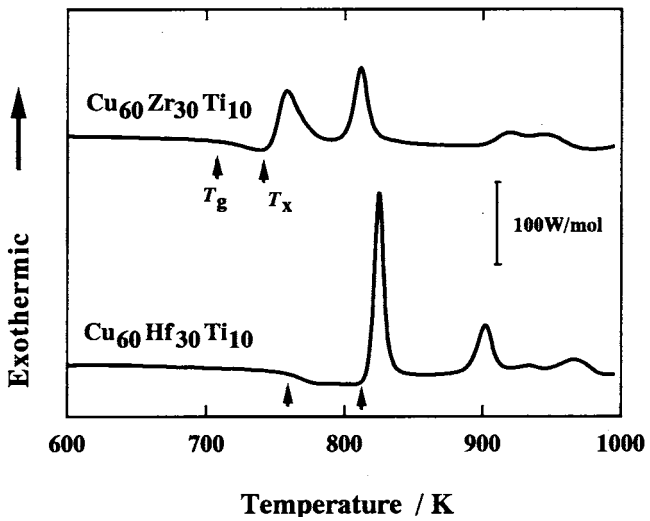

Figure 2. DSC curves of the melt-spun $Cu_{60}Zr_{30}Ti_{10}$ and $Cu_{60}Hf_{30}Ti_{10}$ alloys.

alloy in the XRD patterns. The exothermic reactions with more than three peaks appear after the glass transition in the crystallization process in the DSC curves. The onset temperatures of glass transition, T_g, and crystallization, T_x, are 711 and 745 K in the $Cu_{60}Zr_{30}Ti_{10}$ alloy and 755 and 813 K in the $Cu_{60}Hf_{30}Ti_{10}$ alloy, respectively. The supercooled liquid region defined by the interval of these temperatures in the $Cu_{60}Hf_{30}Ti_{10}$ alloy (58 K) is wider than that in the $Cu_{60}Zr_{30}Ti_{10}$ alloy (34 K), which implies a difference of stability of supercooled liquid state between the alloys. We can also find the difference in the exothermic reactions in the alloys. The transformation proceeds through the sharp exothermic peak at the initial stage in the $Cu_{60}Hf_{30}Ti_{10}$ alloy, which is in contrast to the two exothermic peaks with similar intensities in the $Cu_{60}Zr_{30}Ti_{10}$ alloy. The enthalpy of the first exothermic peak in the $Cu_{60}Hf_{30}Ti_{10}$ alloy is 3.1 kJ mol^{-1}. It is nearly equal to the sum of enthalpies of the first (1.8 kJ mol^{-1}) and second

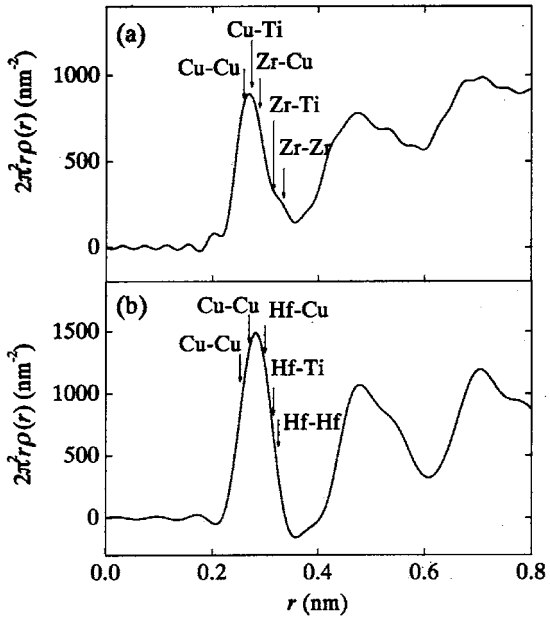

Figure 3. Ordinary RDFs of the melt-spun $Cu_{60}Zr_{30}Ti_{10}$ (a) and $Cu_{60}Hf_{30}Ti_{10}$ (b) alloys.

(1.7 kJ mol^{-1}) peaks in the $Cu_{60}Zr_{30}Ti_{10}$ alloy. The experimental error of the enthalpies is within 5%. The temperature interval between the first and second exothermic peaks of approximately 54 K in the $Cu_{60}Zr_{30}Ti_{10}$ alloy is much smaller than that (approximately 77 K) in the $Cu_{60}Hf_{30}Ti_{10}$ alloy. These results lead to the difference of the transformation behaviour, especially the primary crystallization process, in the present alloys.

For the evaluation of the local structure in the as-quenched samples, XRD measurements are performed. Figures 3(a) and (b) show the RDFs of the melt-spun $Cu_{60}Zr_{30}Ti_{10}$ and $Cu_{60}Hf_{30}Ti_{10}$ alloys, respectively. Both the RDFs have the broad first peak consisting of several atomic pairs and no obvious peaks corresponding to the long-range ordered structure are observed. For the detailed local structure analysis, the AXS measurement was performed in the melt-spun $Cu_{60}Zr_{30}Ti_{10}$ alloy. Figure 4 shows the environmental RDFs around Cu (a) and Zr (b). The environmental RDF around Cu has the broad single first peak, in which the Cu–Cu, Cu–Ti and Cu–Zr pairs overlap due to the similar atomic distances. However, the strong double peaks corresponding to Zr–Cu and Zr–Zr pairs in the environmental RDF around Zr are confirmed. These results imply that the ordered structure in the nanometre scale is formed in the as-quenched state.

In order to examine the nanometre scale ordered structure, HREM observation was carried out. Figure 5 shows the HREM images and selected-area electron diffraction patterns (SADPs) of the as-quenched $Cu_{60}Zr_{30}Ti_{10}$ ((a)–(c)) and $Cu_{60}Hf_{30}Ti_{10}$ ((d)–(f)) alloys, respectively. In the SADPs taken from the region of approximately 1 μm in diameter ((b) and (e)), only the broad rings are observed with no obvious diffraction spots. However, the HREM images ((a) and (d)) exhibit the inhomogeneous structure. The enlarged HREM images in the dark regions ((c) and (f)) have the fringe contrast in the glassy matrix, which indicates the existence of particles with crystalline structure. The crystalline particles have a fine size of approximately 5 nm in diameter and are dispersed randomly. These results are in good agreement with those of the XRD analysis. Thus, it is found that the mixture phases of nanocrystal and glass are contained in the melt-spun $Cu_{60}(Zr \text{ or } Hf)_{30}Ti_{10}$ alloys.

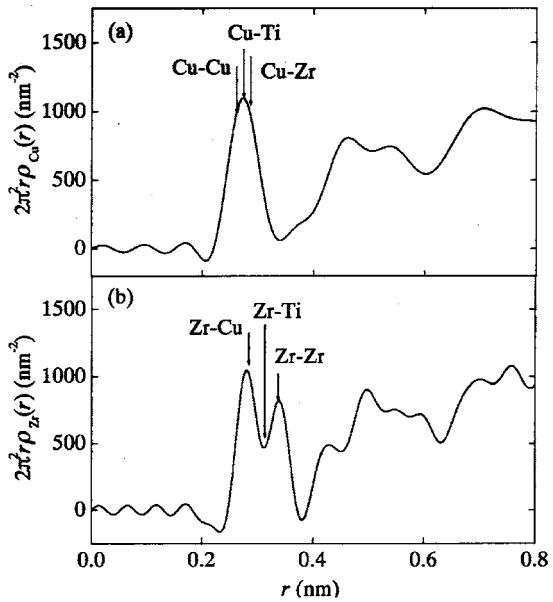

Figure 4. Environmental RDFs of the melt-spun $Cu_{60}Zr_{30}Ti_{10}$ alloy around Cu (a) and Zr (b).

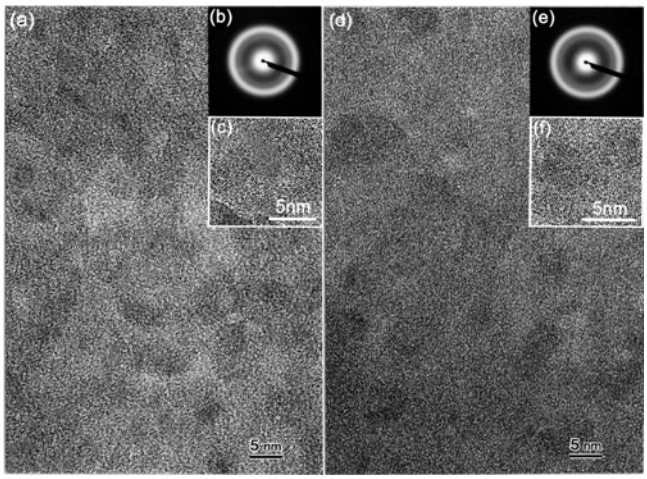

Figure 5. High-resolution electron micrographs (HREMs) and SADPs of the melt-spun $Cu_{60}Zr_{30}Ti_{10}$ ((a)–(c)) and $Cu_{60}Hf_{30}Ti_{10}$ ((d)–(e)) alloys, respectively.

3.2. Characterization of nanocrystalline phase

The HAADF-STEM (Z-contrast) image [11] of the as-quenched $Cu_{60}Zr_{30}Ti_{10}$ alloy is shown in figure 6 for the examination of the atomic deviation in the as-quenched state. The brighter region in the image has relatively high concentration of the heavy atom (Zr) since the thickness is regarded as a constant due to the very small area for HAADF-STEM. The significant compositional segregation, of which the scale is in range of 5–10 nm in diameter, can be observed. A similar image was obtained in the as-quenched $Cu_{60}Hf_{30}Ti_{10}$ alloy. The size of compositional segregation is consistent with the results of HREM observation. It is, therefore, expected that the compositional segregation originates from the structural difference

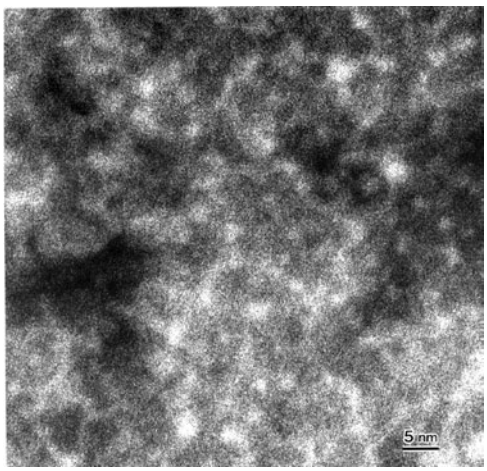

Figure 6. HAADF-STEM (Z-contrast) image of the melt-spun $Cu_{60}Zr_{30}Ti_{10}$ alloy.

Table 1. Nanobeam EDX results of the melt-spun $Cu_{60}Zr_{30}Ti_{10}$ (a) and $Cu_{60}Hf_{30}Ti_{10}$ (b) alloys. (in at.%).

	(a)			(b)		
	Cu	Zr	Ti	Cu	Hf	Ti
Nanocrystal	67.7	26.5	5.8	68.8	26.8	4.4
	71.2	23.5	5.3	64.9	28.7	6.4
	70.9	24.4	4.7	69.0	25.5	5.5
	65.7	28.3	6.0	64.4	29.8	5.8
	68.1	26.0	5.9	70.1	25.4	4.5
Average	68.8	25.7	5.5	67.5	27.2	5.3
Glass	59.3	33.0	7.7	52.7	38.9	8.4
	51.2	39.6	9.2	49.5	41.2	9.3
	54.6	36.9	8.5	53.6	39.7	6.7
	55.0	37.0	8.0	41.7	48.4	9.9
	60.4	31.5	8.1	42.3	48.2	9.5
Average	56.1	35.6	8.3	48.0	43.2	8.8
Whole area (diameter 1 μm)	61.4	30.3	8.3	62.8	29.8	7.4

of nanocrystalline and glassy phases in the as-quenched state of the $Cu_{60}(Zr\ or\ Hf)_{30}Ti_{10}$ alloys. For the determination of the composition of the two phases, nanobeam EDX was performed. The nanobeam EDX results for the nanocrystalline and glassy phases in the melt-spun $Cu_{60}(Zr$ or $Hf)_{30}Ti_{10}$ alloys are summarized in tables 1(a) and (b), respectively. The structure of the analysed region was determined by the nanobeam electron diffraction (NBD) method. The average compositions of five data points in the nanocrystalline and glassy phases are $Cu_{68.8}Zr_{25.7}Ti_{5.5}$ and $Cu_{56.1}Zr_{35.6}Ti_{8.3}$ in the $Cu_{60}Zr_{30}Ti_{10}$ alloy (a) and $Cu_{67.5}Hf_{27.2}Ti_{5.3}$ and $Cu_{48.0}Hf_{43.2}Ti_{8.8}$ in the $Cu_{60}Hf_{30}Ti_{10}$ alloy (b), respectively. It is clarified that the Zr or Hf and Ti atoms are enriched and the Cu element is rejected in the glassy phase.

The structural identification for nanocrystals was examined by NBD. Figure 7 shows the NBD patterns taken from the nanocrystalline particles in the as-quenched $Cu_{60}Zr_{30}Ti_{10}$ ((a), (b)) and $Cu_{60}Hf_{30}Ti_{10}$ ((c), (d)) alloys. The beam diameter for NBD is approximately

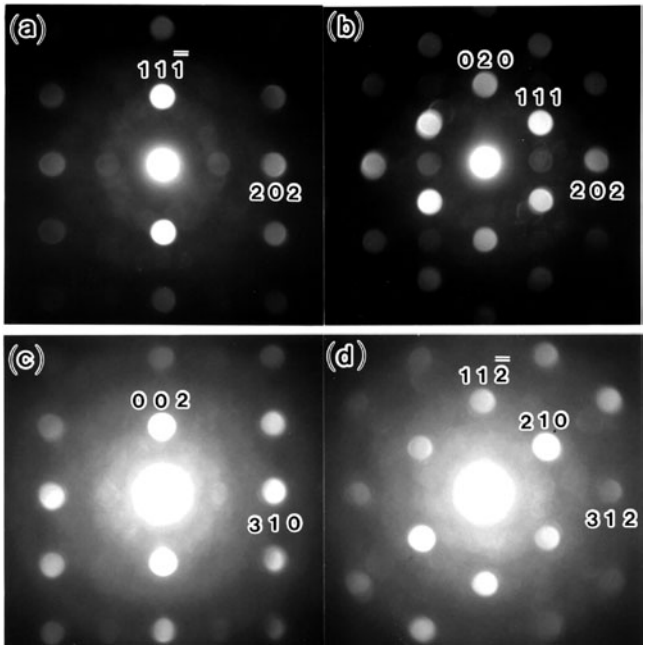

Figure 7. Nanobeam diffraction (NBD) patterns with a beam diameter of 2.4 nm taken from the nanocrystalline particles in the melt-spun $Cu_{60}Zr_{30}Ti_{10}$ ((a), (b)) and $Cu_{60}Hf_{30}Ti_{10}$ ((c), (d)) alloys.

2.4 nm. These patterns are recognized as a cubic structure along the $[1\bar{2}\bar{1}]$ (a), $[10\bar{1}]$ (b), $[1\bar{3}0]$ (c) and $[\bar{2}41]$ (d) zone axes. The lattice constants of the nanocrystalline phases in $Cu_{60}Zr_{30}Ti_{10}$ and $Cu_{60}Hf_{30}Ti_{10}$ alloys are estimated to be $a = 0.45$ and 0.51 nm, respectively. Considering that the Cu content of nanocrystalline particles is approximately 70 at.% and there are no cubic phases in the Cu–Zr, Cu–Hf and Cu–Ti systems with the lattice constants as described above, it is suggested that the cubic structure of Cu-rich nanocrystalline particles is a metastable phase. We can identify that the dark regions (i.e. Zr-poor regions) in the HAADF-STEM image in figure 6 correspond to the nanocrystalline particles with the metastable cubic structure. Therefore, we can conclude that the melt-spun $Cu_{60}(Zr\text{ or }Hf)_{30}Ti_{10}$ alloys have a novel structure consisting of the Cu-rich nanocrystalline particles with the metastable cubic structure in the glassy matrix with a nanoscale compositional segregation.

3.3. Mechanism of the formation of nanocrystalline phase

It is clarified that the glassy phase has comparatively high Zr or Hf and Ti contents in the compositional analysis of the melt-spun $Cu_{60}Zr_{30}Ti_{10}$ and $Cu_{60}Hf_{30}Ti_{10}$ alloys. From the viewpoint of the alloy composition with higher GFA, we prepared the $Cu_{50}Hf_{40}Ti_{10}$ alloy ribbon, which has a similar composition with the glassy region in the melt-spun $Cu_{60}Hf_{30}Ti_{10}$ alloy. The HREM image (a) and SADP (b) of the as-quenched $Cu_{50}Hf_{40}Ti_{10}$ alloy are shown in figure 8. No fringe contrast corresponding to the nanocrystalline particle is observed in the HREM image and it is recognized as the single glassy phase. In the SADP, taken from a region of approximately 1 μm in diameter, only the broad ring is also confirmed with no obvious diffraction spots. These results indicate that no nanocrystalline phase can be formed in the slightly Cu-poor alloy composition deviating from the $Cu_{60}Hf_{30}Ti_{10}$ alloy. It is, therefore realized that the formation of nanocrystalline phase is attributed to an excess of Cu (i.e. a lack

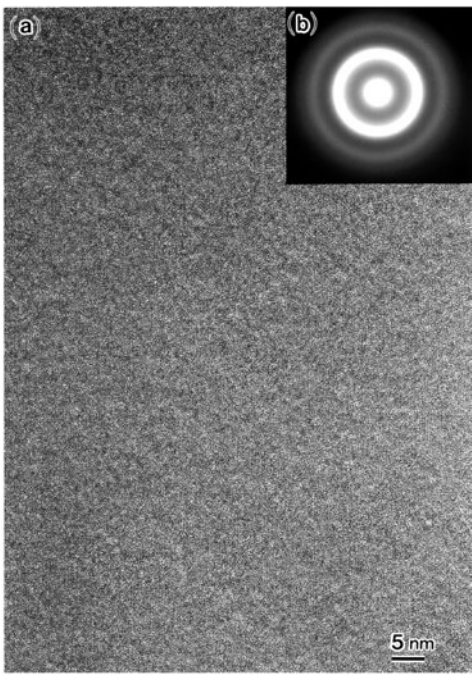

Figure 8. High-resolution electron micrograph (HREM) (a) and SADP (b) of the melt-spun $Cu_{50}Hf_{40}Ti_{10}$ alloy.

of Hf) in the $Cu_{60}Hf_{30}Ti_{10}$ alloy. In contrast, the homogeneous single glassy phase has not been obtained in the $Cu_{50}Zr_{40}Ti_{10}$ melt-spun alloy. Although the reason is still unclear, we suppose that the formation of nanocrystalline phase in the $Cu_{50}Zr_{40}Ti_{10}$ alloy is correlated with the precipitation of metastable bcc CuZr phase. We have found that the CuZr nanocrystalline phase is transformed from the glassy phase in the $Cu_{60}Zr_{30}Ti_{10}$ alloy as discussed below. Considering that the CuZr phase is the metastable phase appearing at high temperature, it may be precipitated easily during the quenching process in the $Cu_{50}Zr_{40}Ti_{10}$ alloy.

We also suggest that the stability of Cu-rich nanocrystalline cubic phase is attributed to the element Ti. Ti has atomic size between Cu and Zr or Hf with the absence of chemical affinities with Zr or Hf, which contributes to the increase of packing density of the cubic phase as well as the glassy phase [12]. This investigation is supported by the increase of number density (i.e. number of atoms in the unit volume) by addition of Ti in the Cu–(Zr or Hf) melt-spun alloy [13]. For example, the number density increases by 1.4% by substituting Ti for 10 at.% Zr in the $Cu_{60}Zr_{40}$ alloy. The calculated number densities in the $Cu_{60}Zr_{30}Ti_{10}$ and $Cu_{60}Zr_{40}$ alloys are 0.0626 and 0.0617 $Å^{-3}$, respectively. The coordination number around Zr in the $Cu_{60}Zr_{30}Ti_{10}$ alloy is approximately 12.8, which is larger than that (10.6) in the $Cu_{60}Zr_{40}$ alloy. These results are also consistent with the investigation of the increase of the packing density by addition of Ti. It is suggested that the high packing density contributes to the suppression of the rearrangement of the constitutional elements, which are one of the main factors for the formation of stable Cu-rich nanocrystalline phases in the as-quenched state [12].

3.4. Primary crystallization

The primary crystallization behaviours of the melt-spun $Cu_{60}(Zr \text{ or } Hf)_{30}Ti_{10}$ alloys containing nanocrystalline particles in the glassy matrix have been investigated by XRD and TEM. Figure 9

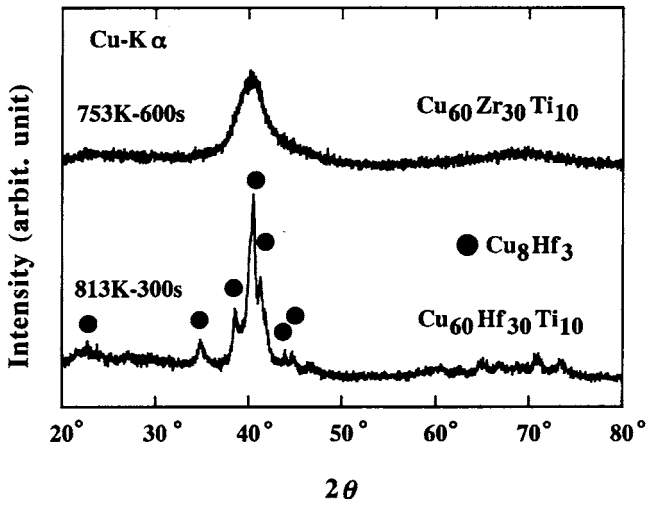

Figure 9. XRD patterns of the $Cu_{60}Zr_{30}Ti_{10}$ alloy annealed for 600 s at 753 K and the $Cu_{60}Hf_{30}Ti_{10}$ alloy annealed for 300 s at 813 K.

shows XRD patterns of the $Cu_{60}Zr_{30}Ti_{10}$ alloy annealed for 600 s at 753 K and the $Cu_{60}Hf_{30}Ti_{10}$ alloy annealed for 300 s at 813 K, which are subjected to the first exothermic reaction in the DSC curves. No obvious diffraction peaks are observed in the annealed $Cu_{60}Zr_{30}Ti_{10}$ alloy, suggesting the precipitation of crystalline phase with a fine grain size. In contrast, the diffraction peaks corresponding to the orthorhombic Cu_8Hf_3 phase are confirmed in the $Cu_{60}Hf_{30}Ti_{10}$ alloy. For further identification of the primary phases, TEM observation was carried out for both the alloys. Figure 10 shows the bright-field TEM images and NBD patterns of the $Cu_{60}Zr_{30}Ti_{10}$ alloy annealed for 600 s at 753 K ((a)–(c)) and the $Cu_{60}Hf_{30}Ti_{10}$ alloy annealed for 300 s at 813 K ((d), (e)). Very fine grains of diameter less than 10 nm are observed in the $Cu_{60}Zr_{30}Ti_{10}$ alloy, which is consistent with the XRD result. The NBD pattern taken from the precipitated particles shown in (b) is identified as a cubic structure along the [111] zone axis with a lattice constant of 0.35 nm. We can realize that the primary precipitation phase has the bcc CuZr structure due to its lattice constant of 0.326 nm. Simultaneously, we obtained the NBD pattern characterized as a cubic structure along the [210] zone axis as shown in (c), which has a lattice constant of 0.53 nm. This lattice constant is similar to that of the Cu-rich nanocrystalline phase in the as-quenched state. These results lead to the suggestion that the glassy phase crystallizes into the bcc CuZr phase leaving the Cu-rich nanocrystalline cubic phase at the first exothermic reaction. It is also consistent with the compositional analysis of the glassy phase in the as-quenched state. The Cu content of the glassy phase is poor (approximately 56 at.%) compared with those of the nanocrystalline phase and the average composition of the whole area in a 1 μm diameter. It is almost equivalent to that of the CuZr phase. The precipitated particles have comparatively large grain size with diameter of 20–50 nm in the $Cu_{60}Hf_{30}Ti_{10}$ alloy shown in (d). The typical NBD pattern in figure 10(e) taken from the particles is identified as the orthorhombic Cu_8Hf_3 phase along the $[0\bar{1}3]$ zone axis, which is in good agreement with the XRD result. Since no NBD pattern corresponding to a cubic phase is obtained in the annealed $Cu_{60}Hf_{30}Ti_{10}$ alloy, it is suggested that the glass and nanocrystalline phases are transformed to the orthorhombic Cu_8Hf_3 phase at the first exothermic reaction in the DSC curve. Therefore, we can summarize the primary

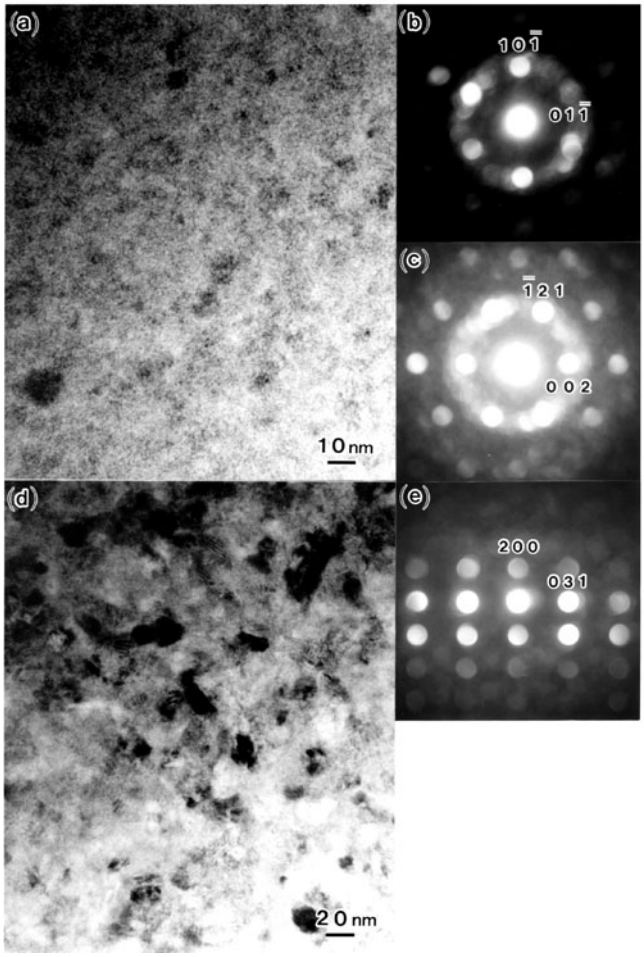

Figure 10. Bright-field TEM images and nanobeam diffraction patterns of the $Cu_{60}Zr_{30}Ti_{10}$ alloy annealed for 600 s at 753 K ((a)–(c)) and the $Cu_{60}Hf_{30}Ti_{10}$ alloy annealed for 300 s at 813 K ((d), (e)).

crystallization process in both the alloys as follows:

glass + nanocrystal (cubic) $\rightarrow$ nano-CuZr + nanocrystal (cubic) in the $Cu_{60}Zr_{30}Ti_{10}$ alloy,

glass + nanocrystal (cubic) $\rightarrow$ nano-Cu_8Hf_3 in the $Cu_{60}Hf_{30}Ti_{10}$ alloy.

It is realized that the difference in the primary crystallization processes between the alloys contributes to the difference in the exothermic reactions in the DSC curves. The large amount of enthalpy of the first exothermic reaction in the $Cu_{60}Hf_{30}Ti_{10}$ alloy is attributed to the transformation of two metastable phases of glass and nanocrystal into the nano-Cu_8Hf_3 phase. Finally, we suggest that the Ti element plays an important role for the formation of nanocrystalline phase in the as-quenched state and nanoscale CuZr or Cu_8Hf_3 phase in the primary crystallization process by the suppression of rearrangement of constitutional elements.

4. Conclusions

It is clarified that the Cu-rich nanocrystalline cubic phases are directly formed during the melt-quenching process in the Cu_{60}(Zr or Hf)$_{30}Ti_{10}$ alloys and the high stability of the Cu-rich

nanocrystalline cubic phases leads to coexistence with the glassy phase in the nanometre scale. The formation of Cu-rich nanocrystalline phase is attributed to the excess of Cu content for the single glassy phase formation. It is also suggested that the Ti element stabilizes the nanocrystalline phases. The primary crystallization phases with a nanometre scale are confirmed. However, we found the difference of the primary crystallization process between the alloys. The nano-bcc-CuZr phase is precipitated with the Cu-rich nanocrystalline phase remaining in the $Cu_{60}Zr_{30}Ti_{10}$ alloy. In contrast, the glassy and Cu-rich nanocrystalline phases are transformed to the orthorhombic Cu_8Hf_3 phase in the $Cu_{60}Hf_{30}Ti_{10}$ alloy at the first exothermic reaction in the DSC curve. These behaviours are also consistent with the difference of the DSC curves in the present alloys.

References

[1] Inoue A, Zhang W, Zhang T and Kurosaka K 2001 *Acta Mater.* **49** 2645
[2] Inoue A 1995 *Mater. Trans. JIM* **36** 866
[3] De Bore F R, Boom R, Mattens W C M, Miedema A R and Niessen A K 1988 *Cohesion in Metals* (Amsterdam: North-Holland) p 361
[4] Inoue A, Zhang T and Masumoto T 1992 *J. Non-Cryst. Solids* **150** 396
[5] Inoue A, Zhang T and Masumoto T 1993 *J. Non-Cryst. Solids* **156–158** 473
[6] Saida J, Li C, Matsushita M and Inoue A 2001 *J. Mater. Res.* **16** 3389
[7] Imafuku M, Sato S, Koshiba H, Matsubara E and Inoue A 2000 *Mater. Trans. JIM* **41** 1526
[8] Wagner C N J, Ocken H and Joshi M L 1965 *Z. Naturf.* a **20** 325
[9] Waseda Y 1980 *Novel Application of Anomalous (Resonance) X-ray Scattering for Structural Characterization of Disordered Materials* (New York: Springer) p 41
[10] Matsubara E, Tamura T, Waseda Y, Zhang T, Inoue A and Masumoto T 1992 *Mater. Trans. JIM* **33** 873
[11] Pennycook S J and Jesson D E 1990 *Phys. Rev. Lett.* **64** 938
[12] Kasai M, Matsubara E, Saida J, Nakayama M, Uematsu K, Zhang T and Inoue A 2002 *Mater. Sci. Eng.* at press
[13] Uematsu K 2002 *Master Thesis* Tohoku University